Proceedings of
10th European Conference on Turbomachinery Fluid dynamics & Thermodynamics
ETC10, April 15-19, 2013, Lappeenranta, Finland

THE UNSTEADY LOW-FREQUENCY AERODYNAMIC FORCES ACTING ON ROTOR BLADES IN THE FIRST TWO STAGES OF A JET ENGINE AXIAL COMPRESSOR IN THE CASE OF A BIRD STRIKE

Romuald Rzadkowski

The R. Szewalski Institute of Fluid Flow Machinery,
Polish Academy of Sciences in Gdansk, Poland
Fiszera 14, 80-952 Gdańsk
z3@imp.gda.pl

Vitally Gnesin, Luba Kolodyazhnaya

National Academy of Sciences of Ukraine, 2/10 Pozharsky st., Kharkov, 61046 Ukraine,
gnesin@ipmach.kharkov.ua

Ryszard Szczepanik

Air Force Institute of Technology, Ksiecia Bolesława 6, 01-494 Warszawa, Poland,
ryszard.szczepanik@itwl.pl

ABSTRACT

A bird strike can cause damage to stationary and rotating aircraft engine parts, especially the engine fan. This paper presents a bird strike simulated by blocking four stator blade passages. It includes the numerical results of the unsteady low-frequency aerodynamic forces and the aeroelastic behaviour caused by a non-symmetric upstream flow affecting the first two rotor blade stages in the axial-compressor of a jet engine.

The applied approach is based on the solution of the coupled aerodynamic-structure problem for a 3D flow through the compressor stages in which fluid and dynamic equations are integrated simultaneously in time. An ideal gas flow through the mutually moving stators and rotor blades with periodicity on the entire annulus is described using unsteady Euler conservation equations, integrated using the Godunov-Kolgan explicit monotonous finite-volume difference scheme and a moving hybrid H-H grid. The structure analysis uses the modal approach and a 3D finite element model of a blade. The blade motion is assumed to be a linear combination of the first natural modes of blade oscillations with the modal coefficients depending on time.

The obtained results show that disturbances in the engine inlet strongly influence the level of unsteady forces acting on the rotor blades. With a partially blocked inlet the whole spectrum of low-frequency harmonics is observed. Such harmonics can lead to rotor blade damage. The low-frequency amplitudes are higher in the first stage rotor blades than in the second stage.

NOMENCLATURE

C damping matrix
F unsteady aerodynamic forces vector
F_{1i} Fourier coefficient
F_{2i} Fourier coefficient
F_y circumferential force
F_z axial force
$h_i = \omega_i \xi_i$
h_y circumferential blade displacement
h_z axial blade displacement
I diagonal matrix
K stiffness matrix
L blade length
M mass matrix
n normal vector
q_i modal coefficient of i-th mode
R_1 first rotor blade
R_2 second rotor blade
U_i displacement vector corresponding to i-th mode shape
v normal velocity
w blade motion vector
z_o number of inlet stator cascade
z_1 number of first stator cascade
z_2 number of second stator cascade
φ torsion blade angle about cross-section gravity center
ξ_i modal damping coefficient
λ modal force
ν 1^{st} harmonic frequency
ρ density
Ω diagonal matrix
ω_i i-th natural blade frequency

INTRODUCTION

Foreign objects entering aircraft engines are a perennial problem. Mathematical analysis and computer simulations can provide information on component stresses already in the design phase.

Foreign objects (e.g. a bird) were characterized as a water-like hydrodynamic response by Wilbeck and Rand [1] in their tests. Storace et al. [2] developed a computer program to predict structural response due to soft body impact. Heidari, Carlson and Yantis [3] developed rotor dynamics as a nonlinear transient analysis for a propulsion system during bird strike induced fan blade loss. Experiments were carried out on SO-3 compressor first stage rotor blades [4] to initiate a crack by placing rectangular blocks on the stator blades, simulating birds engulfed in the engine.

The Fluent code was used to analyze the low frequency excitation caused by inlet blockage of 1.5 stages of an SO-3 engine, but it did not take into account rotor blade vibration Rzadkowski et al. [5], Soliński et al.[6]. Aeroeleastic behaviour of rotor blade 1.5 first compressor stage was analyzed by Rzadkowski et al. [7].

In this paper the unsteady forces acting on rotor blades will be calculated for a 3D non-viscous ideal gas flow through 2.5 compressor stages using an in-house code and taking into account rotor blade vibration.

AERODYNAMICAL MODEL

Blade failures in the first stage of SO-3 compressors were reported in the years 1975-1991 [4]. Experiments were carried out on a first stage rotor blade in an SO-3 engine compressor at the Air Force Institute of Technology in Warsaw to initiate a crack by placing rectangular blocks on the stator blades, which in real life could be caused by birds engulfed in the engine (see Fig. 1a).

The 3D transonic flow of an inviscid non-heat conductive gas through the first compressor stages of an SO-3 aircraft engine was simulated (Fig. 1a).

A 3D whole-annulus model of the first stage of a SO-3 jet engine compressor is shown in Fig. 1b. The model consists of 44 blades in the Inlet Stator Cascade (S0), 28 blades in the Rotor Cascade (R1), 33 blades in the Stator Cascade of the first stage (S1), 42 (R2) rotor blades and 44 (S2) stator blades. The numerical calculations were carried out using computational H-grids (R-Theta-Z):

10*40*84 grid points for the S0 passage, 10*60*78 for the R1 passage, 10*48*68 for the S1 passage, 10*44*64 for the R2 passage and 10*42*62 for the S2 passage.

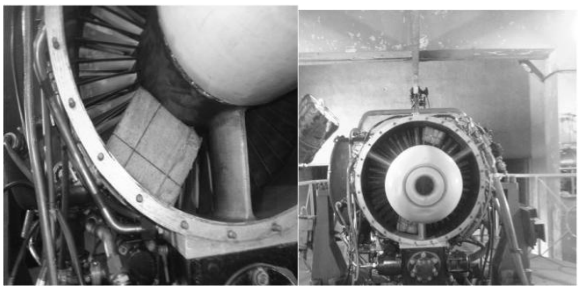

Figure 1a: Test rig of SO-3 engine

In order to model the engine inlet bird strike, four stator blade passages were blocked. Each of the passages is meshed, using an H-type grid for the stators domain and a hybrid H-H grid for the rotor domain ([10], [11]). Here the outer H-grid of the rotor remains stationary during the calculation, while the inner H-grid is rebuilt in each iteration by a given algorithm, so that the external points of the inner grid remain unmoved, but the internal points (on the blade surface) move according to the blade motion. Mesh dependency concerning the fluid- flow and mesh size were analysing in [9], [10].

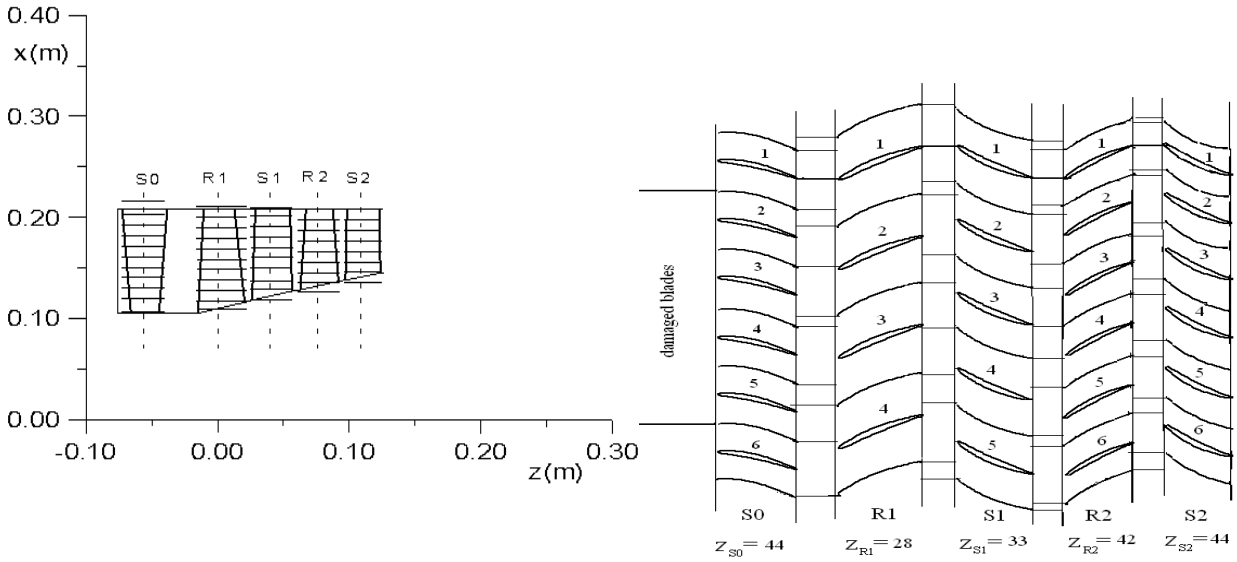

Figure 1b: Computational model of the 2.5 stage (S0-R1-S1-R2-S2)

The spatial transonic flow, including in the general case strong discontinuities in the form of shock waves and wakes behind the exit edges of blades is written in the relative Cartesian coordinate system rotating with constant angular velocity ω according to full non-stationary Euler equations, presented in the form of integral conservation laws of mass, impulse and energy [9]. Wakes were not simulated.

In the general case, when axial velocity is subsonic, at the inlet boundary initial values for total pressure, total temperature and flow angles are used, while at the outlet boundary only the static pressure has to be imposed. Non-reflecting boundary conditions must be used, i.e., incoming waves (three at inlet, one at the outlet) have to be suppressed, which is accomplished by setting their time derivative to zero [9, 10].

On the blade's surface, because the grid moves with the blade, the normal relative velocity is set to zero

$$(v - w)\, n = 0, \tag{1}$$

where: v normal velocity vector, w is blade motion vector, n is normal vector.

STRUCTURAL MODEL

The blade vibration formulation is based on a modal approach of the coupled problem ([11], [12]). The dynamic model of the oscillating blade in linearized formulation is governed by matrix equation:

$$M\ddot{u} + C\dot{u} + Ku = F, \tag{2}$$

where *M*, *C*, *K* are the mass, mechanical damping and stiffness matrices of the blade respectively; *u(t)* is the blade displacement; *F* is the unsteady aerodynamic forces vector, which is a function of blade displacement.

The first step of the modal approach consists of solving the problem of the natural mode shapes and eigenvalues without damping and in a vacuum. Then the displacement of each blade can be written as a linear combination of the first *N* modes shapes with the modal coefficients depending on time:

$$u = Uq = \sum_{i=1}^{N} U_i q_i \tag{3}$$

where U_i is the displacement vector corresponding to i-th mode shape; $q_i(t)$ is the modal coefficient of i-th mode. Taking into account the equation (3) and the orthogonality property of the mode shapes the equation (2) can be written in form of:

$$I\ddot{q} + H\dot{q} + \Omega q = \lambda(t), \tag{4}$$

where I =diag (1, 1, ... 1), H =diag (2 h_1, 2 h_2 , ... 2 h_n), Ω =diag (ω_1^2, ω_2^2 , ... , ω_n^2) are diagonal matrices; ω_i is i-th natural blade frequency; $\{\lambda(t)\}$is the modal forces vector corresponding to the mode shapes, $h_i = \omega_i \xi_i$, where ξ_i is the i-th modal damping coefficient ([11]). Thus the dynamic problem (2) reduces to the set of independent differential equations relatively to modal coefficients of natural modes ([9], [10]):

$$\ddot{q}_i + 2h_i\dot{q}_i + \omega_i^2 q_i = \lambda_i, \tag{5}$$

The equations of motion (5) can be solved using any standard integration method.

The modal forces λ_i are calculated at each iteration with the use of the instantaneous pressure field in the following way ([10]):

$$\lambda_i = \frac{\iint_{\sigma} p\bar{U}_i \cdot \bar{n}^{\circ}\, d\sigma}{\iiint_{v} \rho \bar{U}_i^2\, dv}. \tag{6}$$

where p is the pressure along the blade surface.

NUMERICAL RESULTS

The numerical calculations presented below were carried out for the two and half stages of the SO-3 engine compressor.

The blade vibration was defined by taking into account the first five natural mode shapes of the rotating R1 and R2 blades. The values of natural frequencies are given it Table 1. Mechanical damping was not taken into consideration, becuse we did not have experimental values. Aerodynamical damping was part of the calculation process [10].

Table 1: Natural frequencies of the rotating compressor rotor blades R1, R2

Freq.(Hz)	1	2	3	4	5
Rotor 1	540	1620	2160	3240	4320
Rotor 2	670	2010	2680	4020	6030

The boundary conditions at the inlet and outlet were as follows: the total pressure in absolute system p_o= 101000 Pa, total temperature in absolute system T_o =288 K. In case of the unblocked inlet mass flow was equal to 3.5 kg/s and pressure ratio was 1.67, for the blocked inlet mass flow 19.4 kg/s and pressure ratio 1.69.

The calculation included two regimes. In the first regime the calculations of the unsteady flow through the turbine stage were made by first taking into account the rotor rotation without blade vibration. Next the blades vibration began.

The time step was constant for all the calculated domains and defined by the stability condition of the difference scheme of the linearized equations system [11].

A Fourier analysis was used for the time -dependant numerical results:

$$F(t) = F_0 + \sum_{i=1}^{\infty} F_{1i} \cos(2\pi\nu i t) + F_{2i} \sin(2\pi\nu i t),$$

where F(t) is a physical unsteady load; F_o is the averaged value of load; F_{1i}, F_{2i} are the Fourier coefficients; *i* is the harmonic number; ν is the 1st harmonic frequency. The rotor rotation time was 0.0039 sec and the rotation frequency was 256 Hz.

Unsteady Aerodynamics Forces and Moment

The averaged values of unsteady aerodynamic loads (circumferential, axial forces and moment about the blade cross-section centre of gravity) acting on rotor blades R1, R2 are presented in Tab 2, 3.

Table 2: The averaged values of unsteady loads acting along the R1 blade, blocked inlet, *S0-R1-S1-R2-S2*

L	Fy (N)	Fz (N)	M (N*m)
0.05	-5.131	-1.161	0.0087
0.5	-4.747	-2.414	0.0201
0.95	-4.170	-3.836	0.0231

The average values of circumferential forces were highest in the root, whereas the axial forces and moments were highest in the peripheral blade cross-section**.**

In the case of the blocked inlet, the 4th low-frequency harmonic of circumferential R1 force was the highest in the root cross-section, the 6th harmonic in the 0.55 L cross-section and the 6th harmonic in the 0.96 L cross-section (Fig. 2a).

Table 3: The averaged values of unsteady loads acting along the R2 blade, blocked inlet, *S0-R1-S1-R2-S2*

L	Fy (N)	Fz (N)	M (N*m)
0.05	-5.771	-0.693	0.0089
0.5	-5.484	-2.388	0.0232
0.95	-3.22	-2.809	0.0317

The 5th low-frequency harmonic of axial unsteady force has the highest value in the root cross-section, the 6th harmonic in the 0.55 L cross-section, and the 5th harmonic in the 0.96 L cross-section (Fig. 2b).

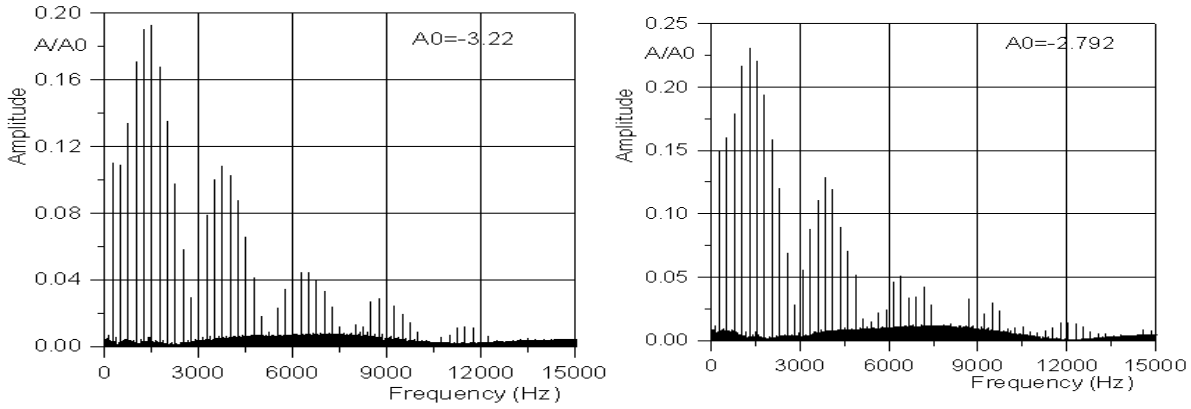

a) **b)**

Figure 2: Amplitude frequency spectrum circumferential F_y and axial force F_z for the peripheral layer of R1 blade

The 5th low-frequency harmonic of circumferential R2 force was the highest in the root cross-section, the 5th harmonic in the 0.55 L cross-section, and the 4th harmonic in the 0.96 L cross-section (Fig. 3a).

The 4th low-frequency harmonic of axial R2 force was the highest in the root cross-section, the 4th harmonic in the 0.55 L cross-section, and the 3th harmonic in the 0.96 L cross-section (Fig. 3b).

Therefore the low frequency unsteady force distributions for R1 and R2 blades are different.

The low frequency harmonics of the R2 blade were smaller (10% of steady part) than those of the R1 blades (22%), but the spectrum of frequencies was similar.

The high-frequency R1 harmonics (ν x z_1 =256×33=8448 Hz), 2% of the steady part and (ν x z_o=256×44=11264 Hz) 1%, where ν was the rotation frequency had smaller values than the low-frequency harmonics.

The high-frequency R2 harmonics (ν x z_1 =256×33=8448 Hz) (5%), (ν x z_o=256×44=11264 Hz and (ν x z_2=256×44=11264 Hz) (1%), where ν was the rotation frequency had smaller values than the low-frequency harmonics, but the difference was smaller than in the case of the R1 blades.

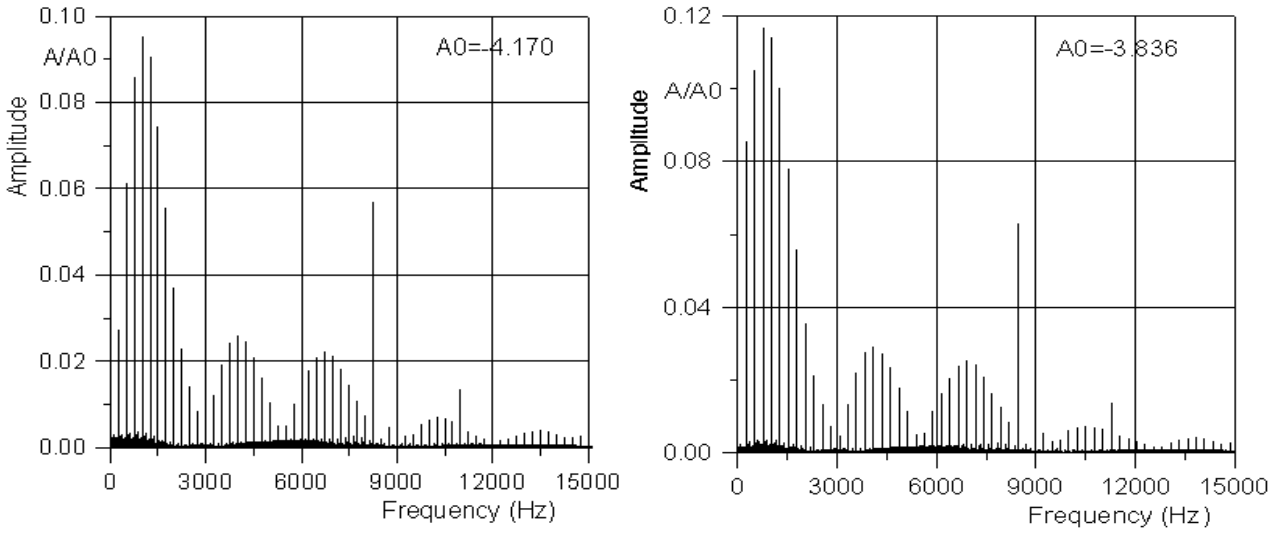

a) **b)**

Figure 3: Amplitude frequency spectrum circumferential F_y and axial force F_z for the peripheral layer of R2 blade

General displacements of rotor blades

In the numerical model R1 and R2 rotor blade vibrations were taken into consideration, hence an aeroelastic analysis was possible.

A comparison between the vibration of rotor blades with and without a blocked inlet is discussed below.

The relative harmonic amplitudes of the R1 blade peripheral layer with an unblocked inlet are presented in Table 4. The first natural frequency of R1 blades was 540 Hz (Tab. 1), so the frequency in the flow decreased to 500 Hz. The unsteady bending of hy components was 6.5% of the average displacements. The amplitudes of torsion vibration (about the blade cross-section gravity center) were 21% of the average twist angle at 450 Hz and 5% at 1800 Hz.

Table 4: Amplitude-frequency spectrum of generalized displacements (hy, hz, φ) of the peripheral blade layer of the R1 blade, unblocked inlet, (*S0-R1-S1-R2-S2)*

L	hy (%) 450 Hz	hz (%) 450 Hz	φ(%) 450 Hz	φ(%) 1800 Hz
0.95	6.5	6.3	21	5.0

The relative harmonic amplitudes of the R1 blade peripheral layer with blocked inlet are presented in Table 5. The frequency in the flow is 450 Hz. The unsteady bending of hy components was 9% of the average displacements. The amplitudes of torsion vibration were 300% of the average twist angle at 750 Hz and 2200% at 1500 Hz.

Therefore blocking the inlet causes a greater decrease of rotor blade vibration frequency in the flow than when the inlet is unblocked. In both cases the form of vibration is bending-torsion and different to the 1st mode shape.

Table 5: Amplitude-frequency spectrum of generalized displacements (hy, hz, φ) of the peripheral blade layer of R1 blade, blocked inlet, (*S0-R1-S1-R2-S2)*

L	hy (%) 450 Hz	hz (%) 450 Hz	φ (%) 750 Hz	φ (%) 1500 Hz
0.95	9	10	300	2200

The bending displacement of R1 blades with an unblocked inlet is presented in Figure 4a. This shows that R1 blades vibrate with constant amplitude, which means that they are self-excited.

Figure 4b shows bending displacement of the R1 blades with a blocked inlet. Here the rotor blade vibration amplitude is considerably higher than in the case of the unblocked inlet, but blade amplitude decreases.

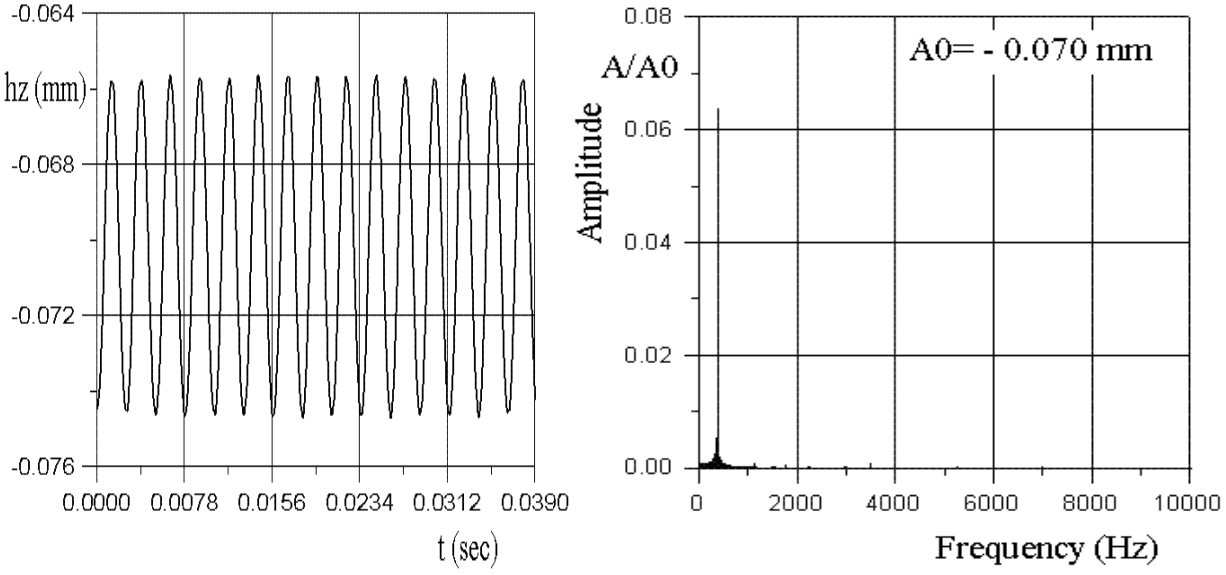

Figure 4a: R1 blade displacement (peripheral layer, axial direction hz), unblocked inlet

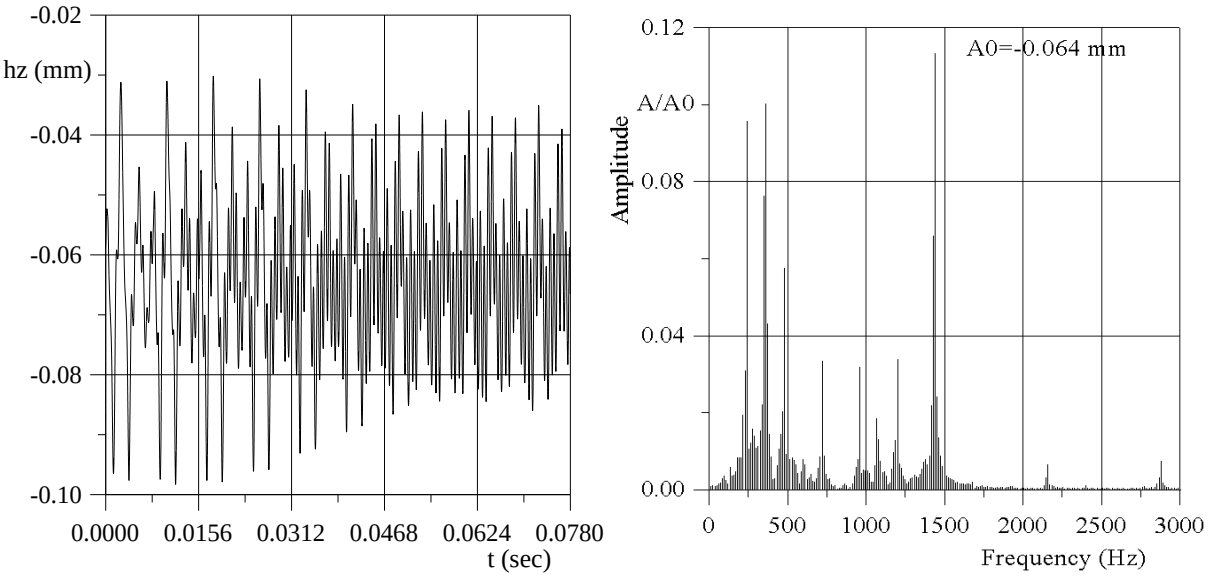

Figure 4b: R1 blade displacement (peripheral layer, axial direction hz), blocked inlet

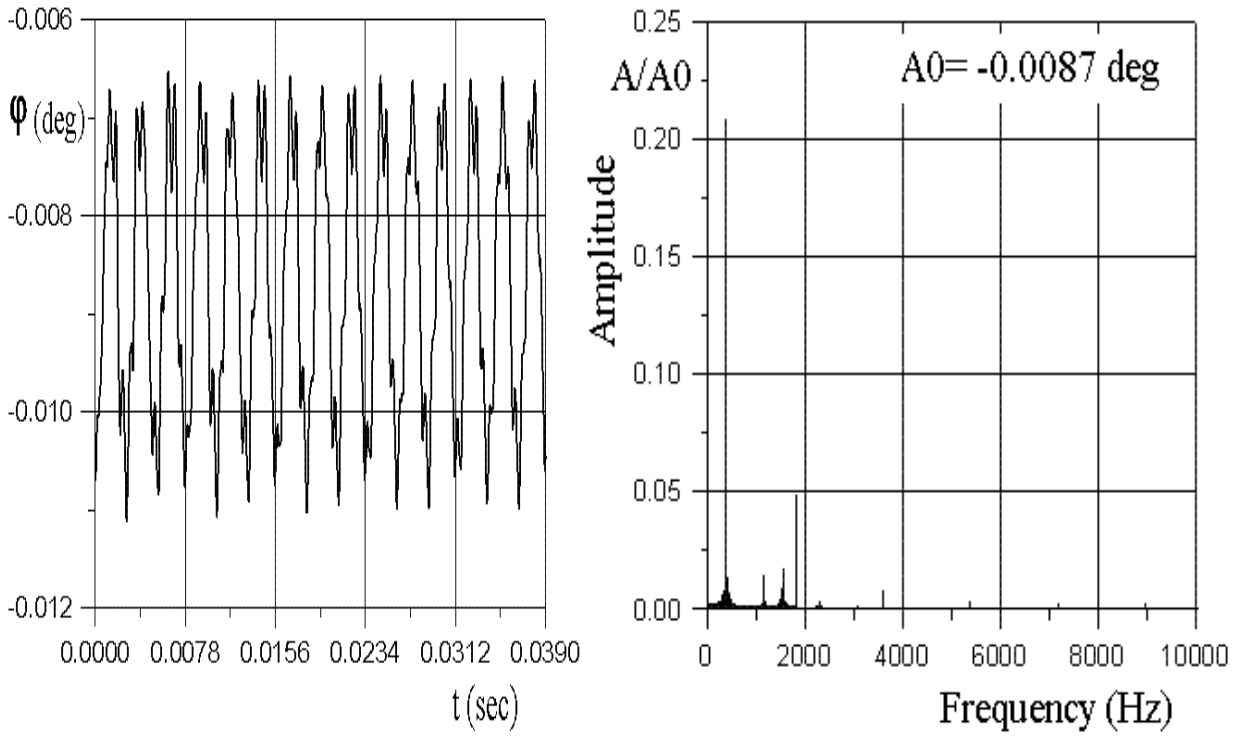

a) **b)**

Figure 5: Amplitude-frequency spectrum of R1 blade torsional oscillations (peripheral layer), unblocked inlet

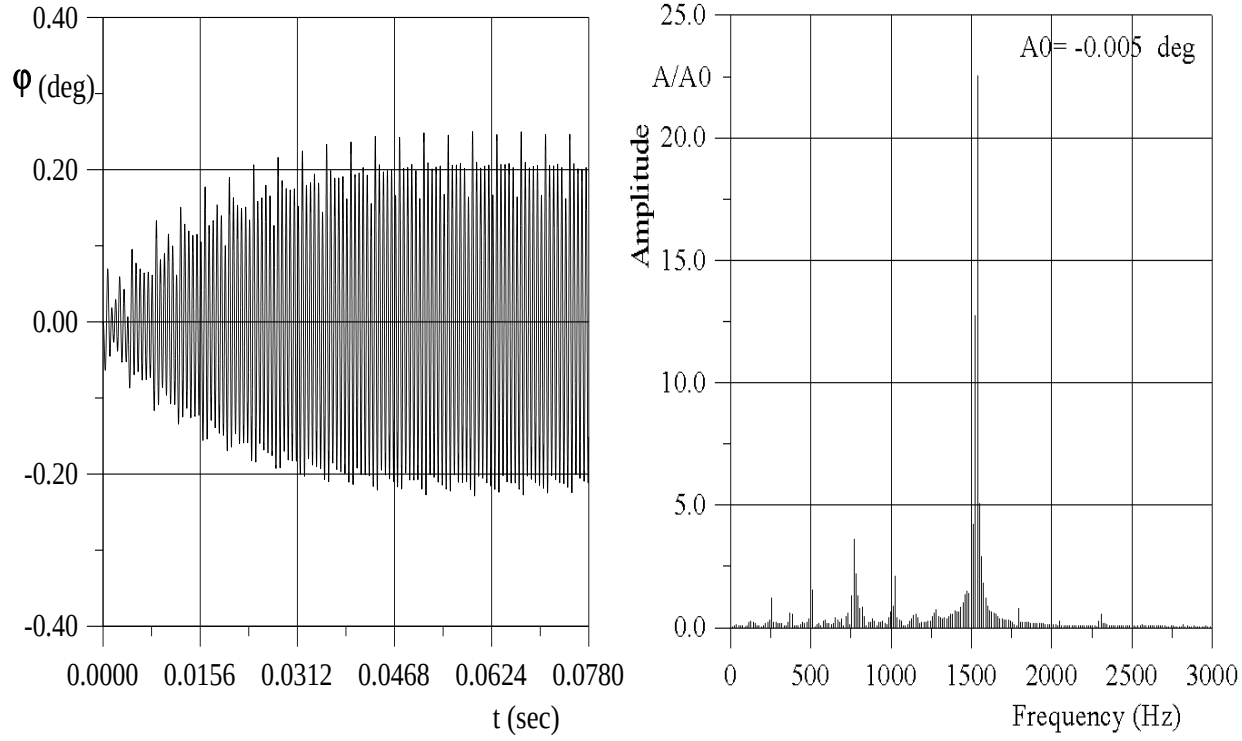

a) **b)**

Figure 6: R1 blade angle (peripheral layer), blocked inlet

The torsion angle of R1 blades with an unblocked inlet is presented in Fig. 5. This shows that R1 blades vibrate with constant amplitude, which means that they are self-excited.

Fig. 6 shows the torsion angle of R1 blades with a blocked inlet. Here the rotor blade vibration amplitude is considerably higher than in the case of the unblocked inlet. This shows that R1 blades vibrate with constant torsional amplitude, which means that they are self-excited. R1 blades with a blocked inlet vibrated with a complex bending–twisting form, bending. This form of vibration is different to the 1st mode shape of the R1 blade.

The relative harmonic amplitudes of the R2 blade peripheral layer with an unblocked inlet are presented in Table 6. The first natural frequency of R2 blades was 670 Hz (Tab. 1), and the frequency in the flow decreased to 450 Hz. The unsteady bending of hy components was 22% of the average displacements. The amplitudes of torsion vibration were 35% of the average twist angle at 450 Hz and 14% at 1500 Hz.

Table 6: Amplitude-frequency spectrum of generalized displacements (hy, hz, φ) of the R2 blade peripheral layer, unblocked inlet, (*S0-R1-S1-R2-S2)*

L	hy (%) 450 Hz	hz (%) 450 Hz	φ(%) 450 Hz	φ(%) 1500 Hz
0.95	22	23	35	14

R2 blades with an unblocked inlet vibrated with a complex bending–twisting form, bending components at 450 Hz and twisting components at 450 Hz and 1500Hz. This form of vibration is different to the 1st mode shape of the R2 blade.

The relative harmonic amplitudes of the R2 blade peripheral layer with blocked inlet are presented in Table 7. The frequency of bending vibration was 450 Hz, the same as for unblocked inlet, although the unsteady component increased to 30%. The frequency of torsion vibration was 450 Hz and the unsteady part was 470%, i.e. higher than the 35% in the case of the unblocked inlet. The second torsional component frequency was 750 Hz and the unsteady part was 270%.

Table 7: Amplitude-frequency spectrum of generalized displacements (hy, hz, φ) of the R2 blade peripheral layer, blocked inlet, (*S0-R1-S1-R2-S2)*

L	hy (%) 450 Hz	hz (%) 450 Hz	φ(%) 450 Hz	φ(%) 750 Hz
0.95	30	32	470	270

Figure 7a shows bending displacement of R2 blades with a blocked and Fig. 7b unblocked inlet. Here the rotor blade vibration amplitude was higher than in the case of the unblocked inlet, in the case we had damping vibration.

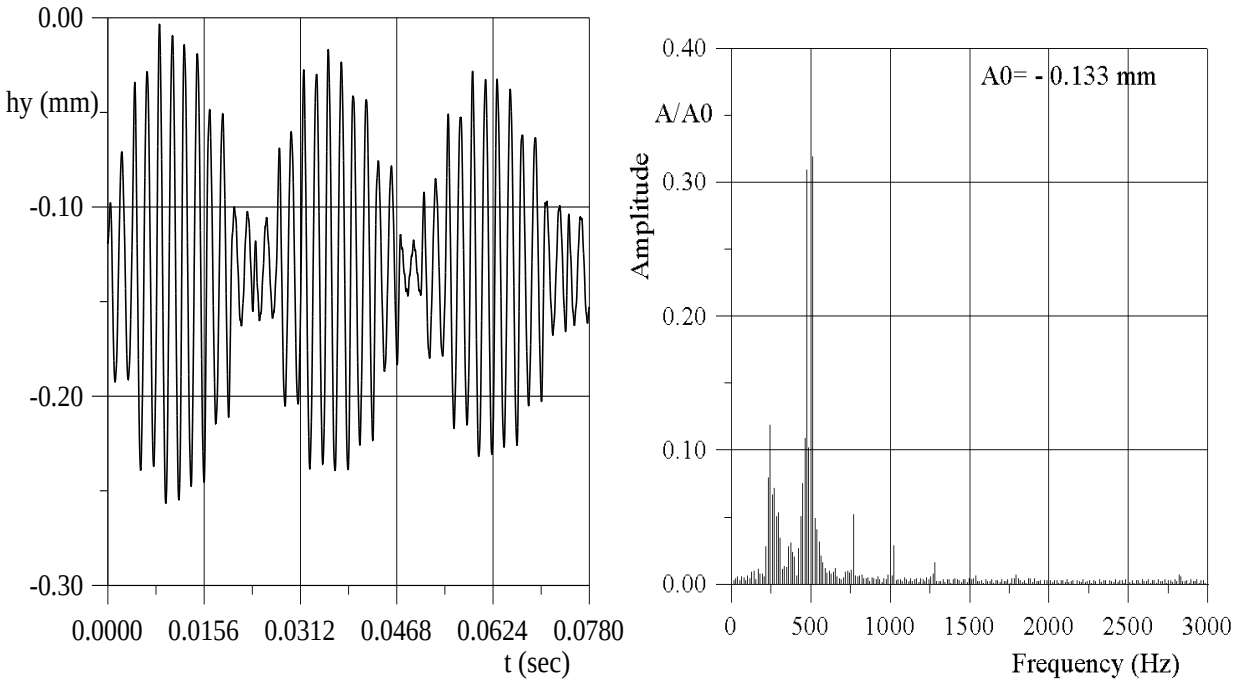

Figure 7a: R2 blade displacement (peripheral layer, circumferential direction hy, blocked inlet)

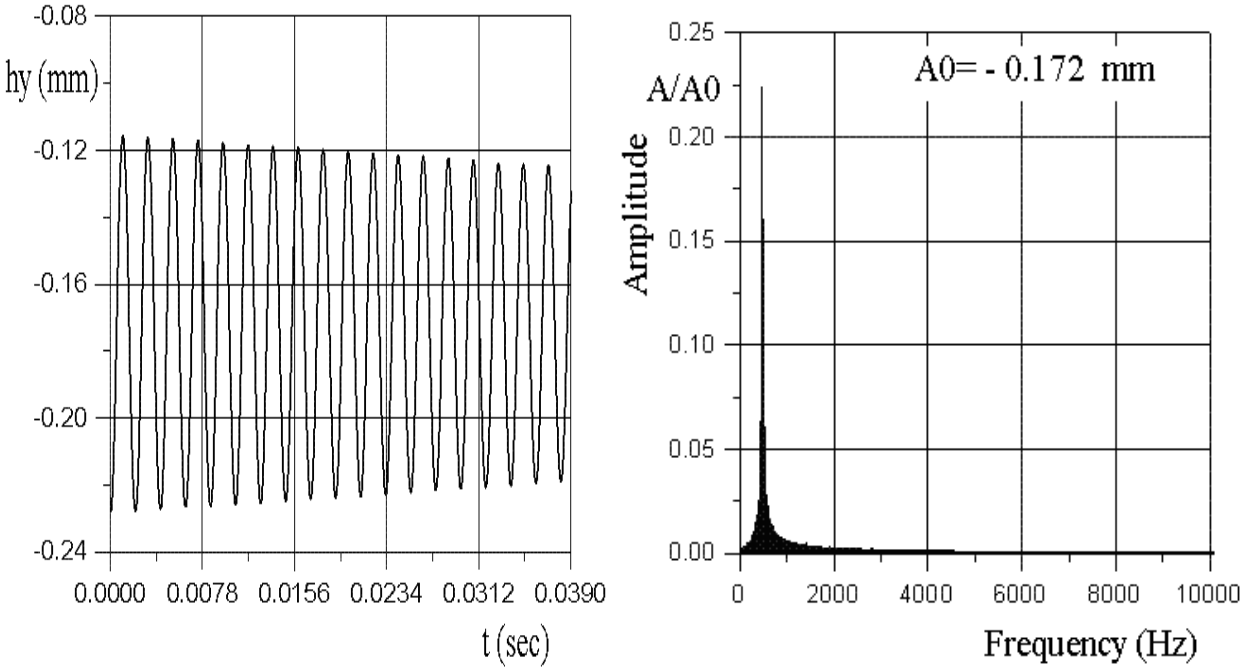

Figure 7b: R2 blade displacement (peripheral layer, circumferential direction hy, unblocked inlet)

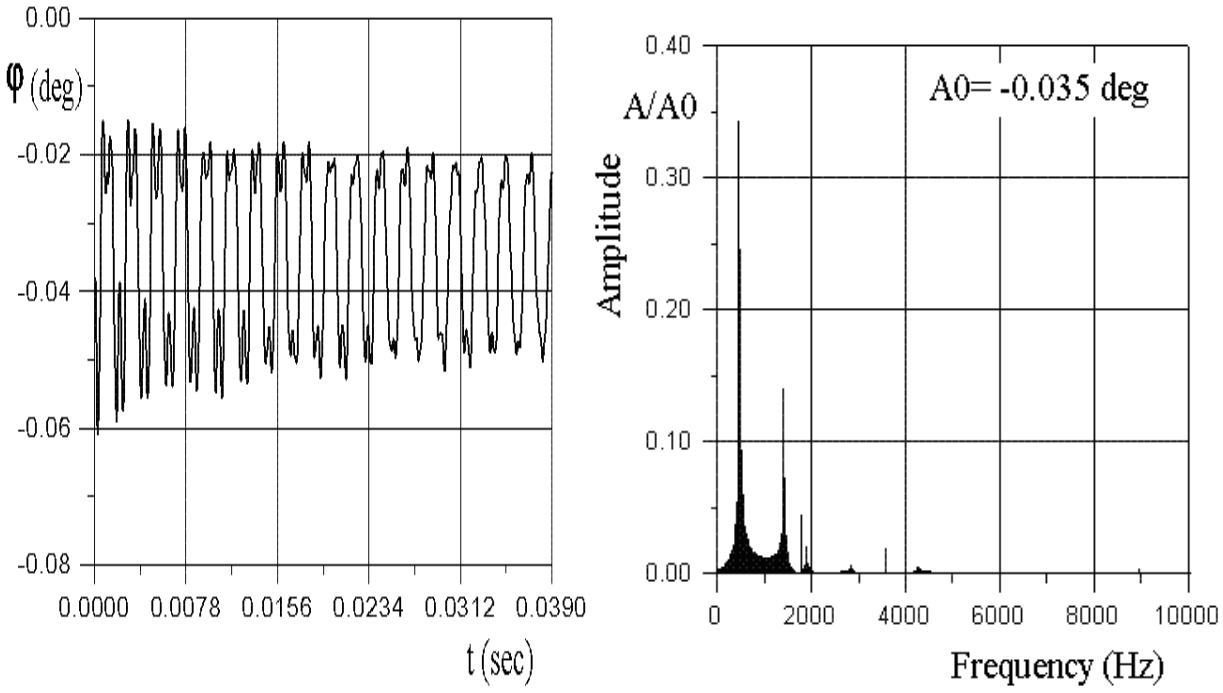

a) **b)**

Figure 8: R2 blade angle (peripheral layer), unblocked inlet

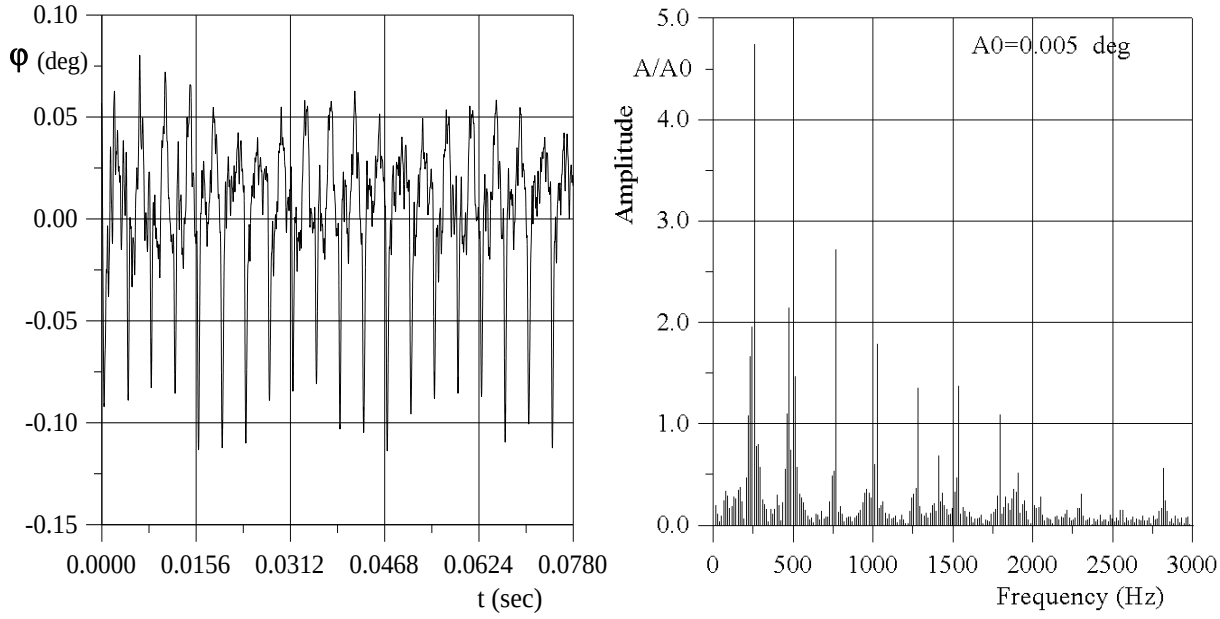

a) **b)**

Figure 9: The amplitude-frequency spectrum of R2 blade torsional oscillations (peripheral layer), blocked inlet

The torsion angle of R2 blades with an unblocked inlet is presented in Figure 8. This shows that R2 blades have damping vibration. Fig. 9 shows the torsion angle of R2 blades with a blocked inlet. Here the rotor blade vibration amplitude was higher than in the case of the unblocked inlet. This means that inlet blockage causes damping vibration with higher amplitude and includes a greater number of torsional components.

CONCLUSIONS

This paper has presented the calculation results for unsteady low-frequency aerodynamic forces acting on SO-3 jet engine compressor R1 and R2 blades, which took into account blade vibration. The forces were analyzed in two operating conditions: with an unblocked and partially blocked engine inlet. The obtained results show that disturbances in the engine inlet strongly influence the level of unsteady forces acting on the rotor blades. With a partially blocked inlet the whole spectrum of low-frequency harmonics was observed, including the natural frequency of blades.

The vibration amplitudes of rotor blades with a blocked inlet are considerably higher than in the case of an unblocked inlet. In this case R1 and R2 blade vibrations differ from their first mode shape and include torsional components.

ACKNOWLEDGMENTS

The authors wish to acknowledge NCBiR (project PBS1/B4/5/2012) for the financial support of this work.

All numerical calculations were made at the Academic Computer Centre TASK (Gdansk, Poland).

REFERENCES

[1] Wilbeck, J. S. and Rand, J. L., The Development of a Substitute Bird Model, Journal of Engineering for Power, ASME, vol. 103, p. 725, 1981.

[2] Storace, A. F., Nimmer R. P. and Ravenhall, R., Analytical and Experimental Investigation of Bird Impact on Fan and Compressor Blading. Journal of Aircraft, Vol. 21, July 1984.

[3] Heidari, M. A., Carlson, D. L. and Yantis, T., Rotor-dynamics Analysis Process, p.3601, Worldwide Aerospace Conference & Technology Showcase, April 8 - 10, Toulouse, 2002.

[4] Szczepanik R., Experimental Analysis of Rotor Blades of Aircraft Engines in Various Operating Conditions, DSc Thesis, ITWL Warsaw, (in Polish) 2010.

[5] Rządkowski R., Soliński M., Szczepanik R., The Unsteady Low-Frequency Aerodynamic Forces Acting on the Rotor Blade in the First Stage of an Jet Engine Axial Compressor, Advances in Vibration Engineering, 11(2), 193-204, 2012.

[6] Soliński M., Rzadkowski R., Pająk A., Szczepanik R., The Unsteady Low-Frequency Forces Acting on the Rotor Blade in the First Stage on an Axial Compressor of SO-3 Jet Engine, Proceedings of the 8th International Conference on Vibration Engineering and Technology of Machinery, VETOMAC –VIII, p. 277-278, Gdansk, Sept 3-6, 2012

[7] Rządkowski R., Gnesin V., Kolodyazhnaya L., Szczepanik R., Aeroelastic Behaviour of First Stage Compressor Rotor Blades with Foreign Object in Engine Inlet, *ISUAAAT'2012, 13TH International Symposium on Unsteady Aerodynamics, Aeroacustics and Aeroelasticity of Turbomachines*, Tokyo, 10-15 Sept, 2012.

[8] Godunov, S., K. et al., Numerical Solution of Multidimensional Problems in Gasdynamicse, Nauka, Moskva, 1976, (in Russian).

[9] Rządkowski R., Gnesin V., 3D Unsteady Forces of the Transonic Flow Through a Turbine Stage with Vibrating Blades, ASME Paper GT-2002-300311, ASME TURBOEXPO 2002, Amsterdam, (June 3-6, 2002) 2002.

[10] Gnesin V., Kolodyazhnaya L., Rzadkowski R., A Numerical Model of Stator-Rotor Interaction in a Turbine Stage with Oscillating Blades, Journal of Fluids and Structures, 19(8), 1141-1153, 2004.

[11] Bathe K., Wilson E, Numerical Methods in Finite Element Analysis, Prentice-Hall, Inc Englewood Cliffs, New Jersey, 1976.

[12] Rządkowski, R., Dynamics of Steam Turbine Blading, Part Two Bladed Discs, Ossolineum, Wrocław-Warszawa, 1998.